J Mater Sci

Energy materials

Water-assisted formation of highly conductive silver nanowire electrode for all solution-processed semi-transparent perovskite and organic solar cells

Xue Sun[1,2,3], Wusong Zha[3], Tong Lin[3], Junfeng Wei[3], Irfan Ismail[3], Zhenguo Wang[3,4], Jian Lin[3], Qun Luo[3], Changzeng Ding[3], Lianping Zhang[3], Zisheng Su[1,*], Bei Chu[1], Dongyu Zhang[3,*], and Chang-Qi Ma[3,4,*]

[1] *State Key Laboratory of Luminescence and Applications, Changchun Institute of Optics, Fine Mechanics and Physics, Chinese Academy of Sciences, Changchun 130033, People's Republic of China*

[2] *University of Chinese Academy of Sciences, Beijing 100039, People's Republic of China*

[3] *Printable Electronics Research Center, Suzhou Institute of Nano-Tech and Nano-Bionics, Chinese Academy of Sciences, 398 Ruoshui Road, SEID, SIP, Suzhou 215123, People's Republic of China*

[4] *Suzhou Institute of Nano-Tech and Nano-Bionics Nanchang, Chinese Academy of Sciences, 298 Luozhu Road, Nanchang 330200, People's Republic of China*

Received: 22 February 2020
Accepted: 13 June 2020

ABSTRACT

Transparent conductive electrode (TCE) is an essential part of modern opto-electronic devices. Silver nanowire (AgNW) is regarded as the most promising TCEs, owing to its balanced conductivity and transparency, and solution processability. The use of insulating polyvinyl pyrrolidone (PVP) surfactant limits the conductivity of the final AgNW networks. Herein, by introducing a small amount of deionized water into the AgNWs dispersion in isopropanol (IPA), the conductivity of the spray-coated AgNW electrode was significantly improved. Sheet resistance (Rs) of 27.0 Ω $\square^{-1}$ with transparency of 92% (at 550 nm) was obtained for the AgNW films spray coated from the AgNW ink with 20% water, which is much lower than the IPA-only AgNW film (120.9 Ω $\square^{-1}$ with similar transparency). Morphology analysis confirmed that water is able to wash PVP away from the AgNW surface and promote the formation of AgNW bundles, which increase the conductivity. The optimized AgNW ink was then used for perovskite and polymer solar cells. High power conversion efficiencies of 14.04% for perovskite solar cell and 6.44% for organic solar cells with averaged light transmittance of 21.7% and 33.12% are achieved, respectively, which are among the highest values for all solution-processed semi-transparent perovskite and polymer solar cells.

Address correspondence to E-mail: suzs@ciomp.ac.cn; dyzhang2010@sinano.ac.cn; cqma2011@sinano.ac.cn

https://doi.org/10.1007/s10853-020-04975-y

Published online: 20 July 2020

Introduction

Transparent conductors play an essential role in modern optoelectronic devices, such as touch screens [1], solar cells [2–5], light-emitting diodes (LED) [6], field-effect transistors (FET) [7], and wearable electronics [8–10]. Indium tin oxide (ITO) has been used as a standard transparent electrode for decades, owning to both excellent electrical conductivity and high optical transmittance [11]. Unfortunately, ITO has unsolvable issues such as poor flexibility, raw material scarcity of supply, and high fabrication cost [12–14]. Thus, various transparent conductors have been developed in the last few years, including conducting polymers [15, 16], carbon materials [17–19], metal grids [20, 21], and metal nanowires [22–24]. Among them, metal nanowires are the most representative materials and have captured much attention, owing to their advantages of high flexibility, high transparency, and ease of fabrication [10]. Applications of AgNW electrode in solar cells [25], light-emitting diodes [26], and wearable electronics [27] have been reported. Although an individual silver nanowire has good electrical conductivity along the wire direction, high junction resistance between nanowires limits the overall conductivity of the final AgNW films [22]. In order to reduce the sheet resistance (Rs) of AgNWs film, various post-treatments, such as thermal heating [28], Joule heating [8], electrochemical coating [22, 29], electron beam irradiation [30], mechanical pressing [31], and plasmonic welding [23], have been developed. However, these methods require either high processing temperature or specific apparatus, leading to a more complicated processing procedure, as alternatives, solvent or chemical welding, such as water immersion [32, 33], silver–ammonia–glucose solution immersion [29], sodium halide salts (such as NaF, NaCl), aqueous solution immersion [34, 35], are simple and cost-efficient approaches to achieve high conductivity of the AgNW film. However, these methods require AgNWs to be exposed to solvents or chemical solutions, making them unsuitable for the preparation of top electrode for electronic devices with sensitive functional layers, such as perovskite solar cells.

Very recently, we reported the preparation of all-solution-processed semi-transparent perovskite solar cells with inkjet-printed AgNW top electrode [36]. By introducing the thin PEI layer, solvent-induced chemical corrosion of AgNW by perovskite film was successfully suppressed, and a high power conversion efficiency of 14% was obtained for the transparent perovskite solar cells. In comparison with inkjet printing, spray coating displays advantages of ease of large-scale production and much fast coating speed. However, the spray coating AgNW thin film typically showed lower conductivity with poorer homogeneity, owing to the nonuniform AgNW droplets [25]. Further decrease in the sheet resistance can be achieved by increasing the content of AgNWs, which will reduce the light transparency. The Haacke figure of merits (FOM) defined as $\Phi_{TC} = T^{10}\ Rs^{-1}$ [37], where T denotes the light transparency and Rs denotes the sheet resistance, is in order of 10^{-3} $(\Omega\ \square^{-1})^{-1}$. An additional thin ZnO layer is required to cover the AgNW electrode to achieve a high conductivity of AgNW electrode, and a PCE over 11% was achieved for the cell with spray-coated transparent AgNW/ZnO top electrode [25]. In this paper, we provide a simple and effective method to improve the conductivity of spray-coated AgNW films by mixing the AgNW dispersion with a small amount of deionized water (DI) into the isopropanol (IPA) solution. The relative slow evaporation rate of water leads to higher water content in the late stage of the drying process. The residual water washes the insulating PVP out of the AgNWs surface and concentrates the PVP component at the edge of the droplet, which forms large AgNW bundles and improves the interconnection between AgNWs. In the meanwhile, the high surface tension of water enhances the capillary force of the water bridge over two silver nanowires and consequently pushes these two silver nanowires together. Both effects improve the interaction between AgNWs and consequently improve the conductivity of the AgNW film. Since no harsh post-treatment requires for this AgNW films, this type of AgNW ink can be directly deposited onto the functional thin layers. Semi-transparent perovskite solar cells with spray-coated AgNW top electrode were demonstrated with a high power conversion efficiency (PCE) of more than 14% with averaged light transparence (AVT) of 21.7%, and a PCE of 6.44% with an AVT of 33.12% for all solution-processed semi-transparent organic solar cell was also achieved.

Experimental section

Materials

The AgNWs dispersed in IPA with a concentration of 10 mg mL^{-1} were purchased from Gu's New Materials co. Ltd. The average diameter and length of these AgNW are 27 nm and 15 μm, respectively. The poly(3,4-ethylenedioxythiophene): poly-(styrene sulfonate) (PEDOT: PSS Clevios PVP AI 4083) was purchased from Heraeus Precious Metals GmbH & Co. KG. $PbCl_2$ (99%), methylammonium iodide (CH_3NH_3I) (99.5%), and PbI_2 (99%) were purchased from Xi'an Polymer Light Technology Corp. Phenyl-C61-butyric acid methyl ester ($PC_{61}BM$) was purchased from Solarmer Energy, Inc. (Beijing). Branched polyethyleneimine (PEI, Mn = 2.5 × 104 g mol^{-1}) was purchased from Sigma-Aldrich. Poly[(2,6-(4,8-bis(5-(2-ethylhexyl-3-chloro)thiophen-2-yl)-benzo[1,2-b:4,5-b′]dithiophene))-alt-(5,5-(1′,3′-di-2-thienyl-5′,7′-bis(2-ethylhexyl)benzo[1′,2′-c:4′,5′-c′]dithiophene-4,8-dione)] (PBDB-T-2Cl) and 3,9-bis(2-methylene-((3-(1,1-dicyanomethylene)-6,7-difluoro)-indanone))-5,5,11,11-tetrakis(4-hexylphenyl)-dithieno[2,3-d:2′,3′-d′]-s-indaceno[1,2-b:5,6-b′]dithiophene (IT-4F) were purchased from Solarmer Energy, Inc. (Beijing). MoO_3 ink was synthesized following the literature reports [38]. Patterned ITO glass was purchased from Shenzhen South China Xiangcheng Technology Co., Ltd. The water-containing AgNW dispersions were prepared by diluting the concentrated AgNW IPA dispersion with a certain amount of water and IPA. The final concentration of AgNW dispersion is 1.2 mg mL^{-1}. The AgNW dispersion was named as AgNW-x, where x denotes the volume ratio of water to the total volume of solvent. For example, AgNW-0 means the AgNW dispersion with pure IPA solvent, while AgNW-20 means the AgNW dispersion with 20% (v/v) of water and 80% (v/v) of IPA.

Fabrication and characterization of the AgNW films

The AgNW dispersions with or without water were spray coated onto glass substrates with a spray coater (Hizenith AC300-1, Hizenith Robot (Suzhou) Co., Ltd.) at a back pressure of 28 Pa. During the spray coating process, the substrates were kept on a hot plate of 53 °C to speed up the evaporation of IPA. By adjusting the nozzle moving speed from 4 mm s^{-1} to 20 mm s^{-1}, AgNW films with different AgNW densities (25.0–5.0 μg cm^{-2}) can be obtained, which show difference in sheet resistance. After that, the glass/AgNW samples were further thermal annealed at 130 °C for 10 min. After cooled down to room temperature, sheet resistance and light transparency of the coated AgNW films were then measured by a four-point probe station (Suzhou Jingge Electronic Co., Ltd) and a UV–visible spectrometer (Lambda 750, PerkinElmer), respectively. Atomic force microscopy (AFM) measurements were recorded by using a Dimension ICON Scanning Probe Microscope at ambient temperature. Scanning electronic microscope (SEM) measurements were used by Quanta 250 FEG under test voltage about 5 kV, and energy-dispersive X-ray spectroscopy (EDS) was measured simultaneously by EDAX APOLLO 10.

Preparation of perovskite solar cells with spray-coated top AgNW electrode

Patterned ITO glasses were cleaned as the previous report [39]. Before the deposition of the hole transporting interface layer, the ITO glasses were treated with ultraviolet ozone for 30 min. A commonly used hole transport material PEDOT:PSS layer was spin coated onto ITO glass at 3500 revolutions per minute (rpm) for 45 s; during this process, 40 μL dimethyl sulfoxide (DMSO) was dropped onto the spinning substrate at 9th second. After that, the substrate was moved to 130 °C hot plate and annealed for 10 min in the ambient atmosphere. After that, the sample was transferred into N_2 glove box for the deposition of the following layers. The perovskite precursor solution was prepared by mixing 103.35 mg of CH_3NH_3I, 306.56 mg of PbI_2 and 9.73 mg of $PbCl_2$ in 350 μL Gamma-butyrolactone and 150 μL DMSO. The precursor solution was then stirred at 55 °C overnight. The perovskite layer was then fabricated through an anti-solvent procedure [40]: fully dissolved perovskite precursor solution (50 μL) was dropped onto PEDOT:PSS hole transport layer at 1000 rpm for 10 s and then 4000 rpm for 30 s. Chlorobenzene (CB, 450 μL) was added onto the spinning substrate at 17 s. The as-deposited perovskite precursor film was then thermally annealed at 100 °C for 10 min to fully convert the yellowish precursor film to dark brown perovskite film. For the electron transport layer (ETL), $PC_{61}BM$ was dissolved in CB (20 mg mL^{-1})

and ultrasonic treated for 2 h. After the perovskite film cooled down to room temperature, $PC_{61}BM$ solution was spin coated on it at 1000 rpm for 45 s. For semi-transparent solar cells, PEI was dissolved in IPA (1 mg mL^{-1}), ultrasonic treated for 2 h, and then spin coated onto $PC_{61}BM$ at 5000 rpm for 60 s to improve the connection between $PC_{61}BM$ and AgNW [25]. AgNW-0 and AgNW-20 were spray coated on the top of the devices at a nozzle moving speed of 16 mm s^{-1}. After that, the solar cells with spray-coated AgNW electrodes were annealed at 85 °C for 5 min. For reference opaque perovskite solar cell, 100-nm-thick Al was thermal evaporated directly on the top of $PC_{61}BM$ under a vacuum of 10^{-5} Pa. The active areas of these perovskite solar cells with both Al and AgNWs as top electrodes are 0.04 cm^2 defined by a photomask for solar simulator measurements.

Preparation of organic solar cells with spray-coated top AgNW electrode

The inverted organic solar cells were prepared on UV ozone-treated ITO, which were the same as the perovskite solar cells mentioned above. A 30-nm-thick ZnO interlayer was deposited through spin coating method at 3000 rpm for 50 s and followed by thermal treating at 140 °C for 10 min in the air. For the photoactive layer, PBDB-T-2Cl and IT4F were dissolved in CB with the ratio of 1:1 (with a total concentration of 20 mg mL^{-1}), and a 0.5% volume ratio of 1,8-diiodooctane was used as the additive. The photoactive layer was deposited on the ZnO layer by spin coating at 2200 rpm for 50 s and heated at 100 °C for 10 min in the glove box. Then, a 10-nm-thick MoOx anode buffer layer was spin coated on the photoactive layer at 2000 rpm for 50 s. Both AgNW-0 and AgNW-20 were increased concentration to 2.5 mg mL^{-1} to achieve higher conductivity; then, the AgNW inks were two consecutively spray coated on the top of the devices at a nozzle moving speed of 16 mm s^{-1}, respectively. After that, the solar cells with spray-coated AgNWs electrodes were annealed at 85 °C for 5 min. The same as perovskite solar cell, 100-nm-thick Al was thermal evaporated directly on the top of MoO_3 under a vacuum of 10^{-5} Pa to form the reference opaque organic solar cell. The active areas of these organic solar cells with different top electrodes are 0.04 cm^2 defined by a photomask for solar simulator measurements.

Characterization of solar cells

The current density–voltage (*J–V*) characters of the perovskite and organic solar cells were measured with a Keithley 2400 source meter in N_2 glove box under a simulated sun AM 1.5 G (Newport VeraSol-2 LED Class AAA Solar Simulator). The external quantum efficiencies (EQE) were tested in a setup, where a 150-W tungsten halogen lamp (Osram 64642) was used to provide probe light. Before passing the monochromator (Zolix, Omni-l300), the light was modulated with a mechanical chopper to select the wavelength. The response was recorded as the voltage by an *I–V* converter (QE-IV Convertor, Suzhou D&R Instruments), using a lock-in amplifier (Stanford Research Systems SR 830).

Result and discussion

Conductivity and transmittance of the AgNWs films

Figure 1a depicts the sheet resistance (Rs) of the spray-coated AgNW films from different AgNW inks. As seen here, the spray-coated AgNW-0 films showed an averaged Rs of 120.9 Ω $\square^{-1}$ with an AVT of 90.8%. By introducing 10% of DI water into the AgNW ink, the spray-coated AgNW-10 films showed a reduced averaged Rs of 47.5 Ω $\square^{-1}$. This was further reduced to 27.0 Ω $\square^{-1}$ with the increase in water content to 20%, while keeping almost the same AVT of 91%. Further increment in water content up to 60% increases the sheet resistance to 30–40 Ω $\square^{-1}$; however, these numbers are still much lower than that of the AgNW-0 films. These results demonstrate that water can increase the conductivity of the coated AgNW film. For the AgNW-70 and AgNW-80 films, the excessive DI water, however, brings poor wettability of the AgNW inks onto the glass surface, leading to high sheet resistance over 1000 Ω $\square^{-1}$ with very poor homogeneity. Interestingly, although the Rs varied obviously with the change of water content in the AgNW inks, negligible change on optical transmittance is observed. As shown in Fig. 1b and Table 1, all these water-containing AgNW films showed high transmittance of around 90% at 550 nm and AVT of 91% over 400 nm and 800 nm, which are almost the same as that of AgNW-0 films. This can be understood by the fact that AgNW densities are

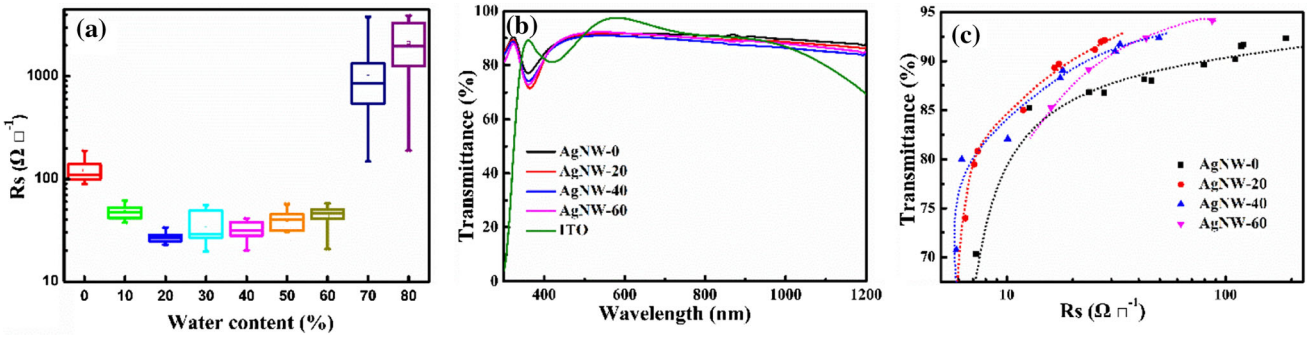

Figure 1 **a** Measured sheet resistance (Rs), transmittance spectra **b** of the AgNW films spray coated from different AgNW-*x* inks at a moving speed of 16 mm s^{-1}; **c** the correlation of Rs and *T* at 550 nm for different AgNW films.

Table 1 Characteristics of AgNW-x films spray coated at a speed of 16 mm s^{-1}

Entry	AgNW ink	Rs (Ω □$^{-1}$)[a]	Transmittance at 550 nm (%)	AVT (%)[b]	$\Phi_{TC} = T^{10}$ Rs^{-1} (Ω^{-1})
1	AgNW-0	120.9 ± 31.6	91.7	90.8	3.16×10^{-3}
2	AgNW-20	27.0 ± 4.2	92.0	90.6	1.37×10^{-2}
3	AgNW-40	31.3 ± 9.8	91.0	89.7	1.07×10^{-2}
4	AgNW-60	43.4 ± 14.1	92.3	90.7	8.73×10^{-3}
5	AgNW-80	2124.5 ± 1796.5	91.2	89.5	1.55×10^{-4}

[a]The calculated average sheet resistance

[b]The average light transmittance over 400–800 nm

identical for all these films (6.2 μg cm^{-2}), since the printing speed was fixed at 16 mm s^{-1} for all samples.

Note that the conductivity of the coated AgNWs electrode can be further increased by reducing the spray nozzle moving speed (increasing the AgNW density). As shown in Figure S1 (in Supporting Information), when spray speed is slowed down to 8 mm s^{-1} (corresponding an increased AgNW density of 12.5 μg cm^{-2}), the average Rs of AgNW-20 films is reduced to 7.1 Ω □$^{-1}$ with an AVT of 79.5%. Further decrease the moving speed can further decrease the sheet resistance down to close to 5 Ω □$^{-1}$. However, the AVT is also significantly reduced to lower than 80% (Table S1 in Supporting Information).

Figure 1c describes the relationship between Rs and T (at 550 nm) of these films spray coated from the AgNW-x inks at different nozzle moving speeds. As seen here, the AgNW-20 and AgNW-40 showed Rs-T curves much closer to the upper left corner when compared to the IPA-only ink (AgNW-0), confirming the positive effect of DI water doping. Table 1 lists the Φ_{TC} of the AgNW-*x* films. As seen here, the AgNW-20 showed a highest Φ_{TC} of 1.37×10^{-2} Ω^{-1}, which is almost an order of magnitude larger than AgNW-0 (3.16×10^{-3} Ω^{-1}) and ITO without post-treatment (2.4×10^{-3} Ω^{-1}) [25]. Nevertheless, by varying the spray coating parameter, conductivity and light transparence of the AgNW films can be tuned by varying the ink formulation and printing processing parameter. More importantly, introducing water into the AgNW ink is helpful for achieving high conductive AgNW electrodes with considerable light transparence.

Morphology of the coated AgNW networks

Figure S3 in Supporting Information shows the optical microscope images of the spray-coated AgNW network films with different water contents. As seen here, with the water content increases, AgNW bundles on the surface become more clearly visible, indicating that water is helpful in formation of AgNW bundles. However, when the water content is greater than 40%, a large number of AgNW bundles formed leading to a significant unevenness of the surface on the 50-micron scale. As a result, the

AgNW-20 exhibits an optimal balance of forming AgNW bundles and film uniformity. To better understand the mechanism of the conductivity improvement in AgNW networks by mixing the AgNW IPA dispersion with water, morphology of the AgNW networks was further investigated by AFM and SEM. Figure 2 depicts the AFM topography (a, b and d, e) and phase (c, f) images of the spray-coated AgNW-0 (a–c) and AgNW-20 (d–f) networks. As seen here, even though silver nanowires are randomly deposited onto the substrate for both samples, round-shaped patterns with a diameter of around 40 μm can be distinguished. Such round-shaped patterns are then considered as the dried droplets of the AgNW ink. Interestingly, the AgNW-20 sample showed more significant round-shaped pattern with big bumps at the edge of the droplet. The zoom-in image (Fig. 2e) shows that such a bump is structureless with visible silver nanowires cross the bump. This demonstrates that the big bump at the edge of the droplet is not the bundles of silver nanowires. Phase image (Fig. 2f) also confirmed that the big bump is different from the silver nanowires in the center of the droplet. Taking it into account that there are only AgNW and PVP in the AgNW ink, we attribute the big bump at the edge of the droplet to the PVP aggregates. The formation of this PVP bump is due to the 'coffee ring effect' of water in the AgNW ink (vide infra). In contrast, the AgNW-0 showed less PVP-rich area over the film. Since both AgNW inks have the same AgNW and PVP concentration, the formation of PVP bumps for the AgNW-20 suggests that there is less PVP in the center area of the dried droplet, when compared to AgNW-0. This conclusion is also supported by the phase images (Fig. 2c, f), where AgNW-20 showed very clear AgNW phases when compared to AgNW-0 film. Interestingly, the averaged surface roughness of AgNW-0 was found to be 19.6 nm, which is similar to that of AgNW-20 (20.5 nm).

Morphology of the spray-coated AgNW films was also investigated by scanning electron microscope (SEM). Figure 3a, d shows the secondary electron (SE) SEM images of AgNW-0 and AgNW-20 films taken in 75 μm scale. Similar to the AFM results (vide supra), edges of the AgNW ink droplet can be clearly

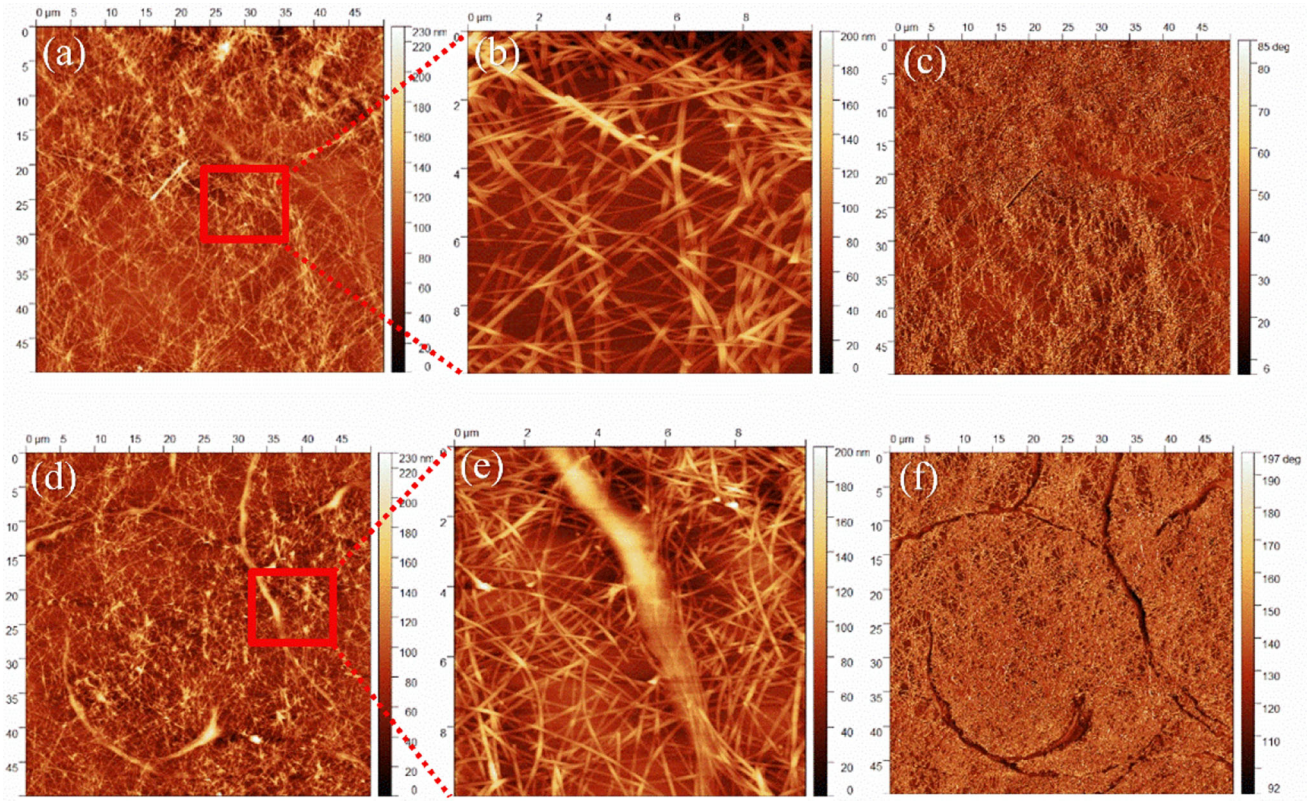

Figure 2 AFM height images under large area scans (**a**, **d**) and local scans (**b**, **e**) of AgNW-0 (**a**, **b**) and **d**, **e** AgNW-20 films; **c**, **f** the phase imagines of the corresponding films.

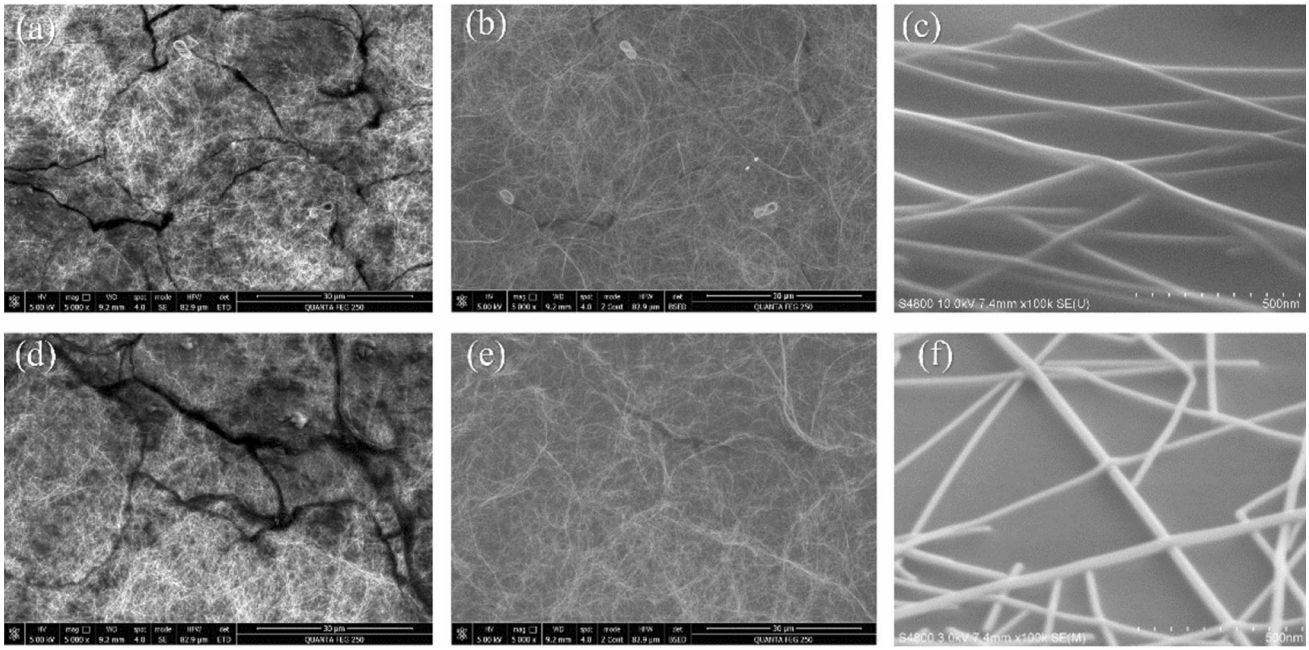

Figure 3 SEM images of AgNW-0 (**a**–**c**) and AgNW-20 (**d**–**f**) films (**b**, **e** are the backscattered electron images of the corresponding films).

seen with dark boundaries. Although EDS measurement did not provide direct evidence of forming PVP domains owing to the low applied voltage during SEM measurement (Figure S4), these dark boundaries in these SEM image are then ascribed to the PVP rich areas, owing to the low conductivity of PVP component. In addition, the AgNW-20 film shows much clear and wider range of droplet boundaries than the AgNW-0 film, indicating that PVP is more intensively concentrated for AgNW-20 film. Also, more bright areas were measured in the center of the AgNW droplet for the AgNW-20 film, indicating that conductivity of the AgNW-20 film is improved when compared to the AgNW-0 film, corresponding well to the conclusion that PVP in the center part of the droplet is partially washed away and then concentrated at the edge of the droplet. Since the SE SEM image gives the topographic information of near-surface layer of the conductive films, to better understand the nanomorphology of the AgNW films, the backscattered electron (BSE) images, where deeper compositional information of the specimen films can be obtained [41], were also measured (Fig. 3b, e). As seen here, the AgNW-20 film has more significant AgNWs bundles than the AgNW-0 film. In addition, larger PVP regions can be still distinguished in the AgNW-0 film (Fig. 3b) than the AgNW-20 film (Fig. 3e), suggesting that there are more PVP aggregates within the AgNW-0 film than AgNW-20 film. In other words, PVP was washed away from AgNWs by water, and the PVP molecules are float on AgNW bundles. The larger AgNW bundles as well as less PVP within the AgNW networks ensure the higher conductivity of the AgNW-20 film. Figure 3c, f shows the zoom-in images of the AgNW-0 and AgNW-20 films. As seen here, AgNWs are rather loosely contacted with others in the AgNW-0 film, whereas the AgNWs are bent to fit the shape of the underlying AgNWs in the AgNW-20 film, suggesting that interaction between AgNWs is improved for the AgNW-20 films.

Drying Process of the water-containing AgNW droplet

Based on the morphology difference of the AgNW-0 and AgNW-20 films, a drying process of the AgNW droplet is proposed as shown in Fig. 4. At the early stage of the drying of ink droplet, the liquid–gas interface at the edge of the droplet is cooler than the bulk. This perturbation of surface temperature induces the surface tension gradients, resulting in a Marangoni flow from edge to center [42]. On the other hand, the high surface tension of water provides a capillary flow from the center to the edge of

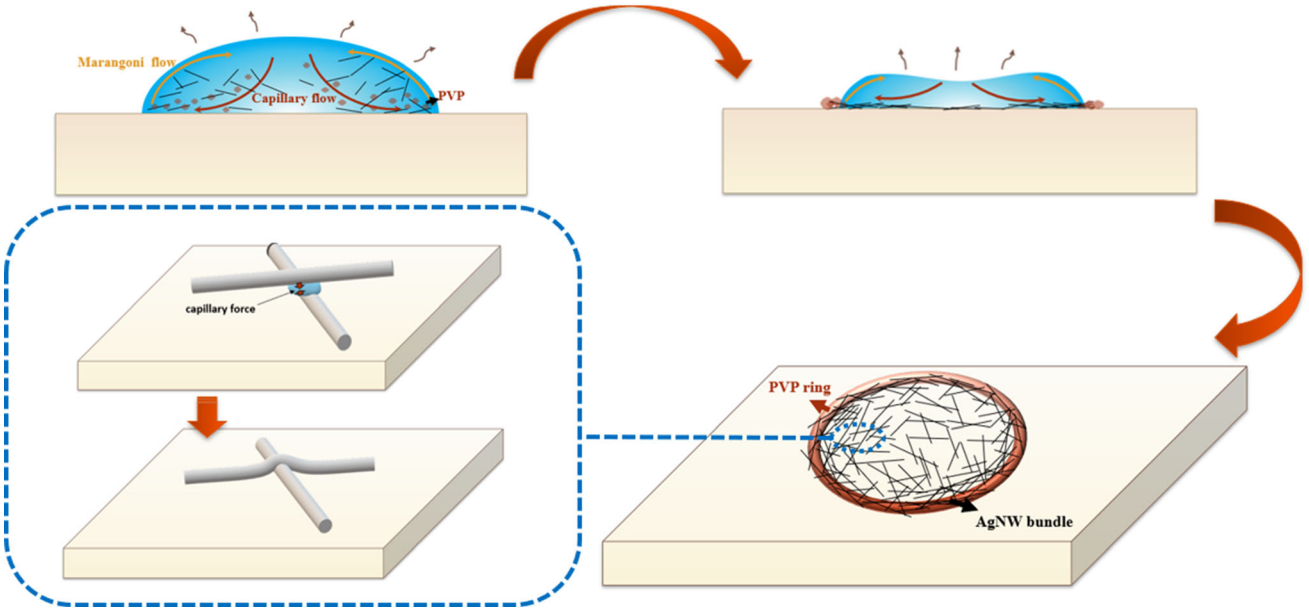

Figure 4 Mechanism for water removed PVP from AgNWs and formed PVP-coated AgNW rings.

the droplet, manifested as an opposite to Marangoni flow [43, 44]. For AgNW-0 droplets, IPA has a relatively low surface tension of 21.7 mN m^{-1} [45], leading to the Marangoni flow plays as the dominant influence in the evaporation process. But for water mixed AgNWs dispersion, the enormous surface tension of water (72.8 mN m^{-1}) [46] significantly enhances the capillary flow over Marangoni flow, resulting in the much-enhanced coffee ring. Since PVP is highly soluble in water, such a capillary flow washes the PVP out from the AgNW surface and is consequently concentrated at the edge of the droplet, leading to the formation of PVP bumps after drying. It is known that the AgNW ink has certain amount of silver nanowires, which means the concentration of PVP is constant, and the process of PVP concentrated at the edge of the droplet lowers the concentration of the center AgNW area and consequently enhances the interconnection of AgNWs, resulting in a cold welding of nanowires.

Meanwhile, since water has a high boiling point than isopropanol, residual water bridges formed between silver nanowires in the final stage of the drying process (Fig. 4), which offers very high capillary force between silver nanowires. This was considered as the most important driving force to bring two AgNWs together [32, 33] that would definitely improve the contact of nanowires. In short summary, reduced sheet resistance of AgNW films from the water-containing AgNW inks is ascribed to the synergistic effect of coffee ring effect of residual water, which washes the insulating PVP from the silver nanowire surface, and the high capillary force of the water bridge between silver nanowires, both of which improves the contact between AgNWs.

Perovskite solar cells with different top electrodes

Preparation of transparent top electrode via solution process for perovskite solar cells is of great interest, since this is the key step for the realization of all solution-processed photovoltaics. AgNWs are considered as the ideal material for use in perovskite solar cells for their high light transparency and excellent conductivity [25]. The current work demonstrates that improved conductivity of the AgNW networks can be achieved by using the water–IPA mixture solvent-based AgNW inks without any harsh post-treatment, making them ideal for using in perovskite solar cells as the top electrode. To confirm this, perovskite solar cells with spray-coated AgNW top electrodes were then fabricated and tested. The perovskite solar cells investigated in this work have a structure of ITO/PEDOT:PSS/$CH_3NH_3PbI_3$/PC_{61}-BM/PEI/AgNW (Fig. 5a), where the AgNW network electrode was prepared by spray coating AgNW-20 on top of the thin PEI layer with a spray speed of 16 mm s^{-1}. For comparison, reference cells with

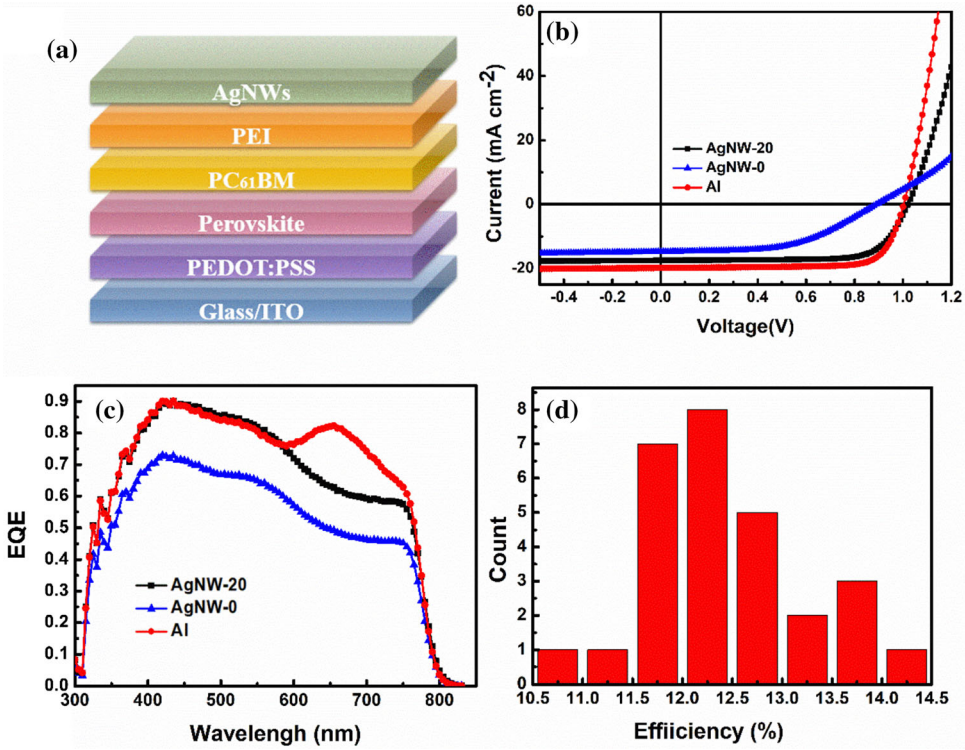

Figure 5 **a** Semi-transmittance perovskite solar cell device structure; **b** *J–V* curves and **c** EQE spectra of the best performance devices with different metal top electrodes; **d** histogram of PCE for 28 individual perovskite solar cells using AgNW-20 as top electrodes.

spray-coated AgNW-0 ink as well as thermal evaporated Al electrodes were also fabricated. A thin layer of PEI was introduced on top of $PC_{61}BM$ to smooth the electron injection from $PC_{61}BM$ to AgNW and to suppress the chemical reaction between perovskite film and silver nanowires [25].

The device with spray-coated AgNW-0 electrode gave poor photovoltaic performance with a low short-circuit current density (J_{SC}) of 14.72 mA cm^{-2}, an open-circuit voltage (V_{OC}) of 0.87 V, a fill factor (FF) of 0.52, and an overall power conversion efficiency (PCE) of 6.78% (Fig. 5b and Table 2), which is similar to our previous result [25]. In contrast, the best AgNW-20-based cell showed a high J_{SC} of 18.60 mA cm^{-2}, V_{OC} of 1.02 V and a high FF of 0.74, leading to an overall PCE of 14.04%, which is more than double the PCE value of the best AgNW-0-based cell. More importantly, greatly improved device reproducibility was found for the AgNW-20-based cells as shown in Fig. 5d. Averaged PCE of these 28 cells is 12.00%, and most of the cells showed high PCE of over 12% (see Figure S5 in the in Supporting Information for more details), demonstrating that AgNW-20 electrode showed much higher device performance in solar cell application. External quantum efficiency (EQE) spectra of these best cells are shown in Fig. 5c; the integral of EQE reflects Jsc of the corresponding device. As seen here, the AgNW-20 cell showed superior photon to electric conversion efficiency over AgNW-0 cell, suggesting much better charge generation and collection within the AgNW-20 cell. In addition, relative lower EQE over 580–800 nm was found for the AgNW-20 cell when compared to the opaque Al cell, which could be

Table 2 Summary of the semi-transparent perovskite solar cells with different metal top electrode photovoltaic properties

Top electrode	Voc (V)	Jsc (mA cm^{-2})[a]	FF	PCE (%)[b]
Al	1.00	20.02	0.77	15.42
AgNW-20	1.02	18.60	0.74	14.04 (12.00 ± 2.04)[c]
AgNW-0	0.89	14.72	0.52	6.78

[a]Jsc is calculated from EQE spectrum

[b]PCE = $V_{oc} \times J_{sc} \times$ FF

[c]averaged data over 28 individual cells

understood by the light transparence of AgNW electrode. The high FF of 0.74 of the AgNW-20 cell is close to that of Al-based cell (0.77), demonstrating a well connection between AgNW-20 and PEI interface layer, which is ascribed to a positive effect of water as well. Overall, such a device performance enhancement can be attributed, on the one hand, to improved conductivity of the AgNW-20 networks as described above and, on the other hand, to improved interface connection between AgNW and $PC_{61}BM$/PEI, since PEI has better solubility in water.

Figure S6(a) in Supporting Information shows the transmission spectrum of the cell over 300–1200 nm wavelength. An averaged light transmittance over 400–800 nm was calculated to be 21.7%, which is among the most efficient semi-transparent perovskite solar cells fabricated by all solution processed (see also S4(b) in the in Supporting Information for the photograph). To fully confirm the semi-transparency of the prepared perovskite solar cells, the photovoltaic performance of the cell illuminated on both ITO and AgNW sides was tested. Figure 6 depicts the *J–V* and EQE curves of the cell with light illumination on different sides, and the photovoltaic performance data are listed in Table 3. Benefiting from the excellent transmittance of AgNW-20 film, the cell performances are also very well when the cell is illuminated on the AgNW side. A PCE of 13.64% with a J_{SC} of 18.13 mA cm^{-2}, V_{OC} of 0.99 V and a high FF of 0.76, which is only 0.4% lower than that illuminated on the ITO side. EQE spectra (Fig. 6b) showed that slightly lower EQE over 300–500 nm was found for the cell illuminated on the AgNW side, which can be ascribed to the low light transmittance of the AgNW film in this wavelength range (Fig. 1b). Interestingly, slightly higher EQE over 500–700 nm was measured for the cell illuminated on the AgNW side, which could be due to the light scattering effect of the AgNWs, leading to the longer light pathways. It is worth also noting that almost no hysteresis was measured for this cell under different illumination sides (Table 3), suggesting there is no obvious charge accumulation at both electrode sides.

Organic solar cells with different top electrodes

Semi-transparent organic solar cells also have great potential for building integrated applications [47]. In order to further verify the application of AgNW-20, we also fabricated semi-transparent organic solar cells with spray-coated AgNW-20 or AgNW-0 as top electrodes. However, initial efforts of using 1.2 mg mL^{-1} AgNW ink for the preparation of organic solar cells gave poor device performance, indicating that organic solar cell is more sensitive to the sheet resistance of the electrode, which could be due to several orders of magnitudes lower charge carrier mobilities ($\sim 10^{-4}$ cm^2 V^{-1} s^{-1}) for the PBDB-T-2Cl:IT-4F blends [48] than that of $CH_3NH_3PbI_3$ ($\sim$ 800 cm^2 V^{-1} s^{-1}) [49]. By increasing the concentration of AgNW ink to 2.5 mg mL^{-1}, we are now able to make good cell by spray coating AgNW top electrode. The structure of bulk heterojunction organic solar cell is described in Fig. 7a. For the devices with AgNW-0 as electrodes, the champion device showed a low V_{OC} of 0.59 V, a Jsc of 8.96 mA cm^{-2}, an FF of 0.35, resulted in an overall PCE of 1.85%. The cells with spray-coated AgNW-20 electrodes show superior performance to the AgNW-0-based cell. The best AgNW-20 cell showed a V_{OC} of 0.84 V, a Jsc of 11.44 mA cm^{-2}, an FF of 0.67, and a noticeable PCE of 6.44%, which is tripled the PCE of AgNW-0-based device (Fig. 7b and Table 4). Owing to the light transparency of the coated AgNW electrode, the J_{SC} of the AgNW-20-based cell is lower

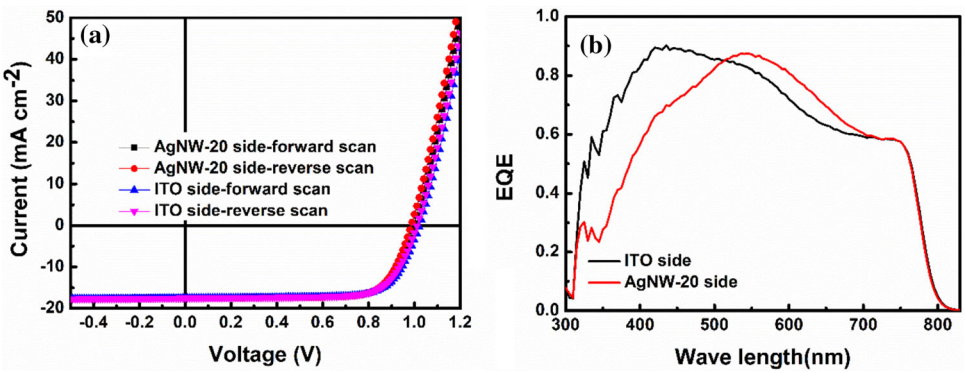

Figure 6 **a** *J–V* curves of the best device illuminated from ITO side and AgNW-20 side, respectively, and **b** the corresponding EQE spectra.

Table 3 Device performances of semi-transparent solar cell illuminate from AgNWs side and ITO side

Illumination direction	*V*oc (V)	*J*sc(mA cm^{-2})[a]	FF	PCE (%)[b]
ITO side—reverse scan	1.02	18.60	0.74	14.04
ITO side—forward scan	1.01	18.65	0.74	13.94
AgNW-20 side—reverse scan	0.99	18.13	0.76	13.64
AgNW-20 side—forward scan	1.00	18.08	0.75	13.56

[a]*J*sc is calculated from EQE spectrum

[b]PCE = $V_{oc} \times J_{sc} \times$ FF

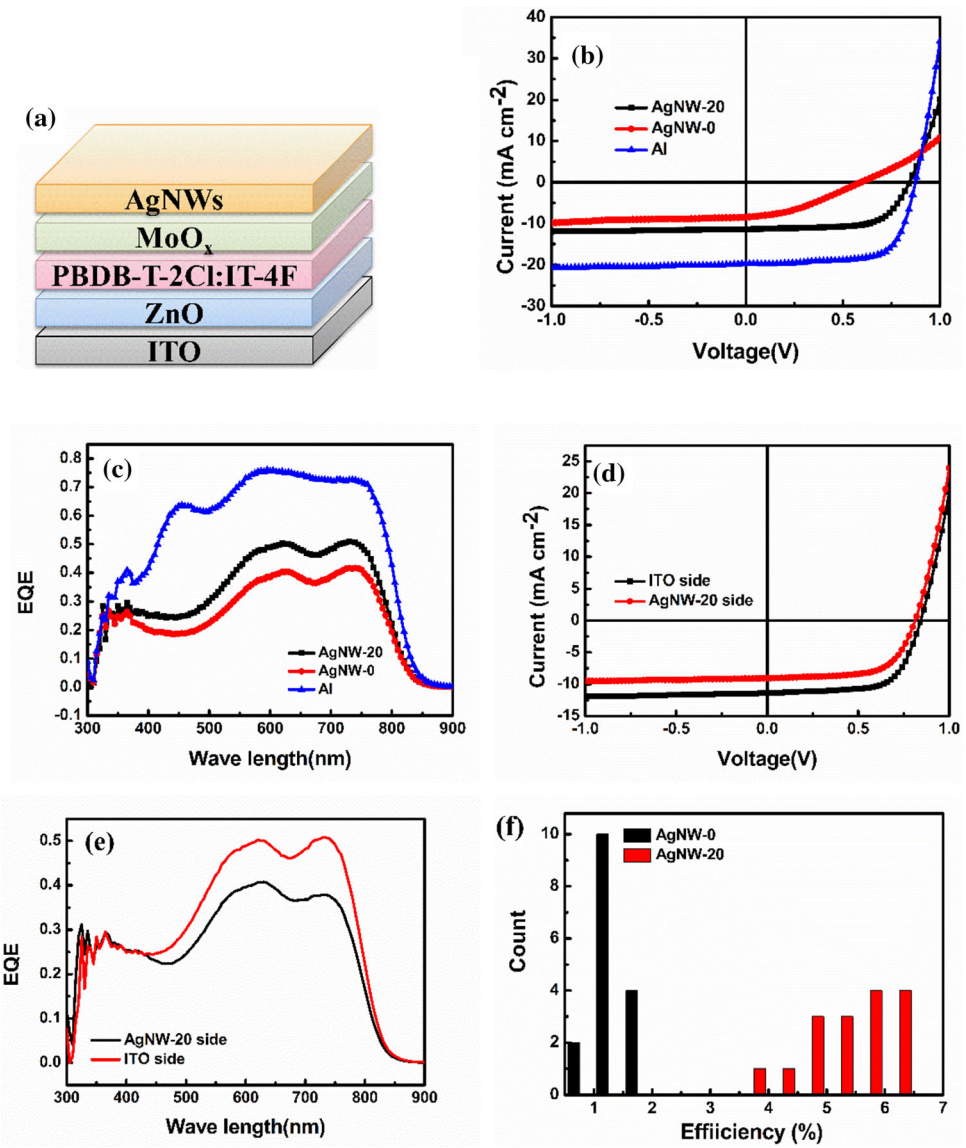

Figure 7 **a** Structure of semi-transmittance organic solar cell device; **b** *J*–*V* curves and **c** EQE spectra of the best performance devices with different metal top electrodes; **d** *J*–*V* curves and **e** the corresponding EQE spectra of the best semi-transparent organic device illuminated from ITO side and AgNW-20 side, respectively; **f** histogram of PCE for 16 individual organic solar cells with AgNW-0 and AgNW-20 top electrodes, respectively.

than that of the opaque cell (11.44 vs. 18.90 mA cm^{-2}), similar to that reported in the literature [47, 50]. However, the V_{OC} and FF are comparable to the opaque Al-based device (V_{OC}: 0.84 vs. 0.88 V, FF: 0.67 vs. 0.70), suggesting that interfacial connection between MoO_3 and AgNW is reasonably good for this fully solution-processed cell. More importantly, the AgNW-20-based cells showed much higher reproducibility than the AgNW-0-based cells, and most of the cells showed PCE of more than 5%

Table 4 Performance parameters of the semi-transparent invert organic solar cells

Top electrode	Illuminated side	*V*oc (V)	*J*sc(mA cm^{-2})[a]	FF	PCE (%)[b]
Al	ITO side	0.88	18.90	0.70	11.64
AgNW-20	ITO side	0.84	11.44	0.67	6.44
AgNW-20	AgNW-20 side	0.81	9.07	0.64	4.74
AgNW-0	ITO side	0.59	8.96	0.35	1.85

[a]Jsc is calculated from EQE spectrum

[b]PCE = $V_{oc} \times J_{sc} \times$ FF

(see Fig. 7f and Figure S7 for more details). The EQE spectra of the champion AgNW-20 and AgNW-0 cells, as well as the reference opaque cell, are shown in Fig. 7c. The relative lower EQE spectra of AgNW-20 and AgNW-0 cells compared to the opaque Al cell could also be understood by the light transparence of AgNW electrodes, while the higher EQE for the AgNW-20 cell than AgNW-0 indicates that charge collection is better in AgNW-20 cell, suggesting that water in AgNW ink is helpful in forming better interfacial connection in polymer solar cells.

Figure S8a in Supporting Information shows the transmission spectrum of the semi-transparent organic solar cell over 300–1200 nm wavelength. An averaged light transmittance (AVT) over 400–800 nm was calculated to be 33.12%, suggesting an excellent light transparency in visible light range (see Figure S8b for the photograph of the semi-transparent organic solar cell). We then test the *J*–*V* characteristics and EQE spectra of the semi-transparent cell illuminated from ITO or AgNW-20 side, and the results are shown in Fig. 7d and e, and the photovoltaic performance data are listed in Table 4. When the cell is illuminated on the AgNW-20 side, a slight lower PEC of 4.74% was obtained with a V_{OC} of 0.81 V, an FF of 0.64, and a J_{SC} of 9.07 mA cm^{-2}, which can be ascribed to light reflectance of the AgNW electrode owing to high AgNW density (25.8 μg cm^{-2}).

Conclusions

In summary, we provide a simple and effective method to improve the conductivity of AgNW films by introducing a small amount of DI water in the AgNWs IPA dispersion. Morphology investigation released that water is able to wash the insulating PVP component from the AgNWs and concentrate PVP at the edge of the droplet, leading to the reduction in PVP concentration in the centre of AgNW networks. In addition, high surface tension of water enhances the capillary force of the water bridge between two AgNWs and consequently brings the two AgNWs in contact to each other. Since no harsh post-treatment is required for forming highly conductive AgNW networks, it is highly suitable for use in sensitive electronic devices as the top electrode. All solution-processed semi-transparent perovskite solar cells having this spray-coated AgNW-20 top electrodes were then fabricated, and a high PCE of 14.04% with an averaged light transmittance of 21.7% was achieved. In addition, all solution-processed semi-transparent organic solar cells with spray-coated AgNW-20 as top electrodes also showed champion PCE of 6.44% and transmittance of 33.12%, which further verify the wide application of AgNW-20.

Acknowledgements

This research was funded through the National Key Research and Development Program of China (Project No. 2017YFB0404501), Natural Science Foundation of Jiangsu Provincial, P. R. China (BK20181197, BE2015071), Jiangxi Provincial Research Program (2018BAB206017).

Compliance with ethical standards

Conflict of interest The authors declare that they have no conflict of interest.

Electronic supplementary material: The online version of this article (https://doi.org/10.1007/s10853-020-04975-y) contains supplementary material, which is available to authorized users.

References

[1] Lee J, Lee P, Lee HB, Hong S, Lee I, Yeo J, Lee SS, Kim TS, Lee D, Ko SH (2013) Room-temperature nanosoldering of a very long metal nanowire network by conducting-polymer-assisted joining for a flexible touch-panel application. Adv Funct Mater 23:4171–4176

[2] Krantz J, Stubhan T, Richter M, Spallek S, Litzov I, Matt GJ, Spiecker E, Brabec CJ (2013) Spray-coated silver nanowires as top electrode layer in semitransparent P3HT:PCBM-based organic solar cell devices. Adv Funct Mater 23:1711–1717

[3] Yu Z, Li L, Zhang Q, Hu W, Pei Q (2011) Silver nanowire-polymer composite electrodes for efficient polymer solar cells. Adv Mater 23:4453–4457

[4] Koppitz M, Wegner E, Rodlmeier T, Colsmann A (2018) Hot-pressed hybrid electrodes comprising silver nanowires and conductive polymers for mechanically robust all-doctor-bladed semitransparent organic solar cells. Energy Technol 6:1275–1282

[5] Czolk J, Landerer D, Koppitz M, Nass D, Colsmann A (2016) Highly efficient mechanically flexible, semi-transparent organic solar cells doctor bladed from non-halogenated solvents. Adv Mater Technol 1:1600184

[6] Fang YS, Ding K, Wu ZC, Chen HT, Li WB, Zhao S, Zhang YL, Wang L, Zhou J, Hu B (2016) Architectural engineering of nanowire network fine pattern for 30 μm wide flexible quantum dot light-emitting diode application. ACS Nano 10:10023–10030

[7] Pang SP, Tsao HN, Feng XL, Mullen K (2009) Patterned graphene electrodes from solution-processed graphite oxide films for organic field-effect transistors. Adv Mater 21:3488–3491

[8] Liang XW, Zhao T, Zhu PL, Hu YG, Sun R, Wong CP (2017) Room-temperature nanowelding of a silver nanowire network triggered by hydrogen chloride vapor for flexible transparent conductive films. ACS Appl Mater Interfaces 9:40857–40867

[9] Bae S, Kim H, Lee Y, Xu XF, Park JS, Zheng Y, Balakrishnan J, Lei T, Kim HR, Song YI, Kim YJ, Kim KS, Ozyilmaz B, Ahn JH, Hong BH, Iijima S (2010) Roll-to-roll production of 30-inch graphene films for transparent electrodes. Nat Nanotechnol 5:574–578

[10] Wang X, Zhi LJ, Mullen K (2008) Transparent, conductive graphene electrodes for dye-sensitized solar cells. Nano Lett 8:323–327

[11] Liang ZM, Graham KR (2015) Surface modification of silver nanowires for morphology and processing control in composite transparent electrodes. ACS Appl Mater Intererfaces 7:21652–21656

[12] Lu H, Ren X, Ouyang D, Choy WCH (2018) Emerging novel metal electrodes for photovoltaic applications. Small 14:1703140

[13] Chung WH, Park SH, Joo SJ, Kim HS (2018) UV-assisted flash light welding process to fabricate silver nanowire/-graphene on a PET substrate for transparent electrodes. Nano Res 11:2190–2203

[14] Lee JY, Connor ST, Cui Y, Peumans P (2008) Solution-processed metal nanowire mesh transparent electrodes. Nano Lett 8:689–692

[15] Vosgueritchian M, Lipomi DJ, Bao ZA (2012) Highly conductive and transparent PEDOT:PSS films with a fluorosurfactant for stretchable and flexible transparent electrodes. Adv Funct Mater 22:421–428

[16] Kim T, Kim YW, Lee HS, Kim H, Yang WS, Suh KS (2013) Uniformly interconnected silver-nanowire networks for transparent film heaters. Adv Funct Mater 23:1250–1255

[17] Wu ZC, Chen ZH, Du X, Logan JM, Sippel J, Nikolou M, Kamaras K, Reynolds JR, Tanner DB, Hebard AF, Rinzler AG (2004) Transparent, conductive carbon nanotube films. Science 305:1273–1276

[18] Zhang M, Fang SL, Zakhidov AA, Lee SB, Aliev AE, Williams CD, Atkinson KR, Baughman RH (2005) Strong, transparent, multifunctional, carbon nanotube sheets. Science 309:1215–1219

[19] Hecht DS, Hu LB, Irvin G (2011) Emerging transparent electrodes based on thin films of carbon nanotubes, graphene, and metallic nanostructures. Adv Mater 23:1482–1513

[20] Wang J, Fei F, Luo Q, Nie SH, Wu N, Chen XL, Su WM, Li YJ, Ma CQ (2017) Modification of the highly conductive PEDOT:PSS layer for use in silver nanogrid electrodes for flexible inverted polymer solar cells. ACS Appl Mater Interfaces 9:7834–7842

[21] Yu S, Han HJ, Kim JM, Yim S, Sim DM, Lim H, Lee JH, Park WI, Park JH, Kim KH, Jung YS (2017) Area-selective lift-off mechanism based on dual-triggered interfacial adhesion switching: highly facile fabrication of flexible nanomesh electrode. ACS Nano 11:3506–3516

[22] Hu LB, Kim HS, Lee JY, Peumans P, Cui Y (2010) Scalable coating and properties of transparent, flexible, silver nanowire electrodes. ACS Nano 4:2955–2963

[23] Park JH, Hwang GT, Kim S, Seo J, Park HJ, Yu K, Kim TS, Lee KJ (2017) Flash-induced self-limited plasmonic welding of silver nanowire network for transparent flexible energy harvester. Adv Mater 29:1603473

[24] Sachse C, Weiss N, Gaponik N, Muller-Meskamp L, Eychmuller A, Leo K (2014) ITO-free, small-molecule organic solar cells on spray-coated copper-nanowire-based transparent electrodes. Adv Energy Mater 4:1300737

[25] Han K, Xie ML, Zhang LP, Yan LP, Wei JF, Ji GQ, Luo Q, Lin J, Hao YY, Ma CQ (2018) Fully solution processed semi-transparent perovskite solar cells with spray coated silver nanowires/ZnO composite top electrode. Sol Energy Mater Sol Cells 185:399–405

[26] Spechler JA, Koh TW, Herb JT, Rand BP, Arnold CB (2015) A transparent, smooth, thermally robust, conductive polyimide for flexible electronics. Adv Funct Mater 25:7428–7434

[27] Liang JJ, Li L, Niu XF, Yu ZB, Pei QB (2013) Elastomeric polymer light-emitting devices and displays. Nat Photon 7:817–824

[28] Song TB, Chen Y, Chung CH, Yang Y, Bob B, Duan HS, Li G, Tu KN, Huang Y, Yang Y (2014) Nanoscale joule heating and electromigration enhanced ripening of silver nanowire contacts. ACS Nano 8:2804–2811

[29] Xiong WW, Liu HL, Chen YZ, Zheng ML, Zhao YY, Kong XB, Wang Y, Zhang XQ, Kong XY, Wang PF, Jiang L (2016) Highly conductive, air-stable silver nanowire@Iongel composite films toward flexible transparent electrodes. Adv Mater 28:7167–7172

[30] Hong CH, Oh SK, Kim TK, Cha YJ, Kwak JS, Shin JH, Ju BK, Cheong WS (2015) Electron beam irradiated silver nanowires for a highly transparent heater. Sci Rep 5:17716

[31] Tokuno T, Nogi M, Karakawa M, Jiu JT, Nge TT, Aso Y, Suganuma K (2011) Fabrication of silver nanowire transparent electrodes at room temperature. Nano Res 4:1215–1222

[32] Zhang K, Li J, Fang YS, Luo BB, Zhang YL, Li YQ, Zhou J, Hu B (2018) Unraveling the solvent induced welding of silver nanowires for high performance flexible transparent electrodes. Nanoscale 10:12981–12990

[33] Liu Y, Zhang JM, Gao H, Wang Y, Liu QX, Huang SY, Guo CF, Ren ZF (2017) Capillary-force-induced cold welding in silver-nanowire-based flexible transparent electrodes. Nano Lett 17:1090–1096

[34] Gu JH, Wang XL, Chen HT, Yang SH, Feng HH, Ma X, Ji HJ, Wei J, Li MY (2018) Conductivity enhancement of silver nanowire networks via simple electrolyte solution treatment and solvent washing. Nanotechnology 29:265703

[35] Kang H, Kim Y, Cheon S, Yi GR, Cho JH (2017) Halide welding for silver nanowire network electrode. ACS Appl Mater Interfaces 9:30779–30785

[36] Xie ML, Lu H, Zhang LP, Wang J, Luo Q, Lin J, Ba LX, Liu H, Shen WZ, Shi LY, Ma CQ (2018) Fully solution-processed semi-transparent perovskite solar cells with ink-jet printed silver nanowires top electrode. Sol RRL 2:1700184

[37] Haacke G (1976) New figure of merit for transparent conductors. J Appl Phys 47:4086–4089

[38] Wang YL, Luo Q, Wu N, Zhu HF, Chen LW, Li YQ, Luo LQ, Ma CQ (2015) Solution-processed MoO3: PEDOT: PSS hybrid hole transporting layer for inverted polymer solar cells. ACS Appl Mater Interfaces 7:7170–7179

[39] Tan MX, Ji GQ, Zhang LP, Wang J, Wang C, Chen Q, Luo Q, Chen LW, Ma CQ (2018) Simultaneous performance and stability improvement of perovskite solar cells by a sequential twice anti-solvent deposition process. Org Electron 59:358–365

[40] Jeon NJ, Noh JH, Kim YC, Yang WS, Ryu S, Seok SI (2014) Solvent engineering for high-performance inorganic–organic hybrid perovskite solar cells. Nat Mater 13:897–903

[41] Vernon-Parry KD (2000) Scanning electron microscopy: an introduction. III-Vs Rev 13:40–44

[42] Mampallil D, Eral HB (2018) A review on suppression and utilization of the coffee-ring effect. Adv Colloid Interfaces 252:38–54

[43] Xiong JQ, Li SH, Ye YY, Wang JX, Qian K, Cui P, Gao D, Lin MF, Chen TP, Lee PS (2018) A deformable and highly robust ethyl cellulose transparent conductor with a scalable silver nanowires bundle micromesh. Adv Mater 30:1802803

[44] Zhong X, Duan F (2016) Flow regime and deposition pattern of evaporating binary mixture droplet suspended with particles. Eur Phys J E 39:18

[45] Cheong WJ, Carr PW (1987) The surface-tension of mixtures of methanol, acetonitrile, tetrahydrofuran, isopropanol, tertiary butanol and dimethylsulfoxide with water at 25-°C. J Liq Chromatogr 10:561–581

[46] Kim D, Jeong S, Park BK, Moon J (2006) Direct writing of silver conductive patterns: improvement of film morphology and conductance by controlling solvent compositions. Appl Phys Lett 89:264101

[47] Ji G, Wang Y, Luo Q et al (2018) Fully coated semitransparent organic solar cells with a doctor-blade-coated composite anode buffer layer of phosphomolybdic acid and PEDOT: PSS and a spray-coated silver nanowire top electrode. ACS Appl Mater Interfaces 10:943–954

[48] Fan Q, Zhu Q, Xu Z et al (2018) Chlorine substituted 2D-conjugated polymer for high-performance polymer solar cells with 13.1% efficiency via toluene processing. Nano Energy 48:413–420

[49] Valverde-Chavez DA, Ponseca CS, Stoumpos CC et al (2015) Intrinsic femtosecond charge generation dynamics in single crystal $CH_3NH_3PbI_3$. Energy Environ Sci 8:3700–3707

[50] Min J, Bronnbauer C, Zhang ZG et al (2016) Fully Solution-processed small molecule semitransparent solar cells: optimization of transparent cathode architecture and four absorbing layers. Adv Funct Mater 26:4543–4550